FULL PAPER

High-Performance Broadband Circularly Polarized Beam Deflector by Mirror Effect of Multinanorod Metasurfaces

Zhaocheng Liu, Zhancheng Li, Zhe Liu, Jianxiong Li, Hua Cheng, Ping Yu, Wenwei Liu, Chengchun Tang, Changzhi Gu, Junjie Li, Shuqi Chen,* and Jianguo Tian**

Manipulation of light phase and amplitude by plasmonic metasurfaces has immensely promising applications in optical imaging, information processing, communications, and quantum optics. However, the controllability of efficiency and bandwidth is relatively low for the single-layer metasurfaces. Here, a high efficiency and broadband circularly polarized (CP) beam deflector based on multirod single-layer metasurfaces is presented. Each unit can be regarded as an imperfect polarizer, and the phase and amplitude induced by the mirror effect can be easily controlled. Owing to the plasmonic hybridization, the high efficiency and broadband characteristics of the proposed metasurfaces are theoretically and experimentally demonstrated. Meanwhile, an easy way to determine the polarization degree of the incident light based on Poincaré sphere is also proved by the multirod metasurfaces. Our work provides a simple alternative way to enhance the efficiency of CP anomalous light and thus has robust applications in nanophotonics and nanooptics.

1. Introduction

Metasurfaces with abrupt phase change have recently exhibited extraordinary light-manipulation abilities, which were found novel applications in flat lenses, spin–orbit manipulation, wavefront engineering, information processing, holography, to name a few. It has been shown that various shaped optical antennas in interface of two media are able to generate phase gradient for scattered light. V-shaped antennas are first demonstrated to enable an abrupt phase discontinuity and gradient of the cross-polarized component supporting anomalous refraction and reflection, governed by generalized Snell's law (GSL).[1–3] Other kinds of optical antennas such as C-shaped antennas and metallic patches were also proved to be able to manipulate wavefront of scattered waves for refracted or reflected light.[4–12] Among these new-type anomalous-scattering devices, the control of circularly polarized (CP) light is testified feasible in both theory and experiment—with spatially various antennas arranged properly. The phase of CP light is modulated without paying attention on scattered intensity generated by each antenna.[13–17]

Harnessing light for modern photonic applications often involves the control and manipulation of light intensity or efficiency. The most important issue for generating anomalous scattered lights is also the efficiency by reasonable arrangement of the various shaped or layered plasmonic metasurfaces. Compared with normal light conforming to ordinary Snell's law, the efficiency of the anomalous scattered lights is far too low in the previous works. Some methods have been proposed to improve the intensity of abnormal light but at the same time suppress that of normal one. For example, plasmonic metasurface can be sandwiched by gratings to increase the efficiency of cross-polarized light with the help of Fabry–Pérot effect;[18,19] or few-layer composite metascreen made of dielectric and metal is used to enhance the performance of control.[20,21] These approaches dramatically enhance the efficiency of anomalous light, but at the same time increase the processes and difficulty in fabrication because of their extra structures (gratings or board) and precise distance between antennas and gratings. However, so far it is still challenging to further improve the efficiency of anomalous light with circular polarization by a single-layer plasmonic metasurface.

Here, we introduce a new approach to describe the function of a polarizer and show an intuitive method to describe the extra phase of CP light due to its orientation. We present the design, fabrication, and characteristics of the multinanorod plasmonic metasurfaces, in which each unit can be regarded as an imperfect polarizer with extraordinary broadband. The high efficiency and broadband effects are theoretically and experimentally demonstrated. The correctness of GSL is also demonstrated by experimental results. At last, arbitrary polarized incidence is considered, and an easy way to determine the polarization degree of the incident light based on Poincaré sphere is feasibly proved by the proposed plamonic metasurfaces.

Dr. Z. Liu, Dr. Z. Li, J. Li, Prof. H. Cheng, Dr. P. Yu, Dr. W. Liu, Prof. S. Chen, Prof. J. Tian
Laboratory of Weak Light Nonlinear Photonics
Ministry of Education, School of Physics
and Teda Applied Physics Institute
Nankai University
Tianjin 300071, P.R. China
E-mail: schen@nankai.edu.cn; jjtian@nankai.edu.cn
Dr. Z. Liu, Dr. C. Tang, Prof. C. Gu, Prof. J. Li
Beijing National Laboratory for Condensed Matter Physics
Institute of Physics
Chinese Academy of Sciences, P.O. Box 603
Beijing 100190, P.R. China
E-mail: jjli@iphy.ac.cn

DOI: 10.1002/adfm.201502046

2. Results and Discussion

A traditional linear polarizer can be regarded as a device, which can absorb and scatter a part of the incident light, and transmit the linearly polarized light. The linearly polarized transmitted light is actually the combination of two opposite-helicity CP lights when the CP light is incident on linear polarizer. Part of incident CP light is converted into opposite-helicity CP light. The orientation of linear polarizer determines the polarized direction of the transmitted light. We adopt the Dirac notation to define the left circularly polarized (LCP) and right circularly polarized (RCP) lights as $|L\rangle = \begin{bmatrix} 1 \\ -i \end{bmatrix}$ and $|R\rangle = \begin{bmatrix} 1 \\ i \end{bmatrix}$, respectively. Considering linear polarizer may be imperfect, we introduce the operator P to generalize the description of linear polarizer as[22,23]

$$P|L\rangle = \alpha|L\rangle + \beta|R\rangle e^{-i2\varphi} \quad (1)$$

$$P|R\rangle = \alpha|R\rangle + \beta|L\rangle e^{i2\varphi} \quad (2)$$

where φ is the orientation angle of linear polarizer. α and β are the actual amplitude transmittance of the scattered lights for original and opposite handedness, respectively. For convenience in analyzing the polarization state of transmitted light, we normalized them in the form of $\alpha + \beta = 1$. **Figure 1**a shows the geometrical interpretation for the imperfect linear polarizer following Equations (1) and (2). When a LCP light with a phase angle ϕ along x-axis interacts with the linear polarizer, a part of incident light is converted into RCP light, forming an elliptically polarized light in transmitted side. Interestingly, the linear polarizer could execute a mirror effect, which symmetrically and partially images the incident light (object), including its helicity and phase, to the opposite-helicity light with the amplitude transmittance of β (image) with respect to the linear polarizer. For a perfect linear polarizer, the converted light (image) has the same amplitude ($\alpha = \beta = 0.5$) as the unconverted light (remained object). The total effect is that a linearly polarized light with orientation angle φ is scattered.

The phase of the image can be tuned by orientation of the linear polarizer. When an array of linear polarizers is linearly rotated along x-axis from 0 to π, the image will have a gradient

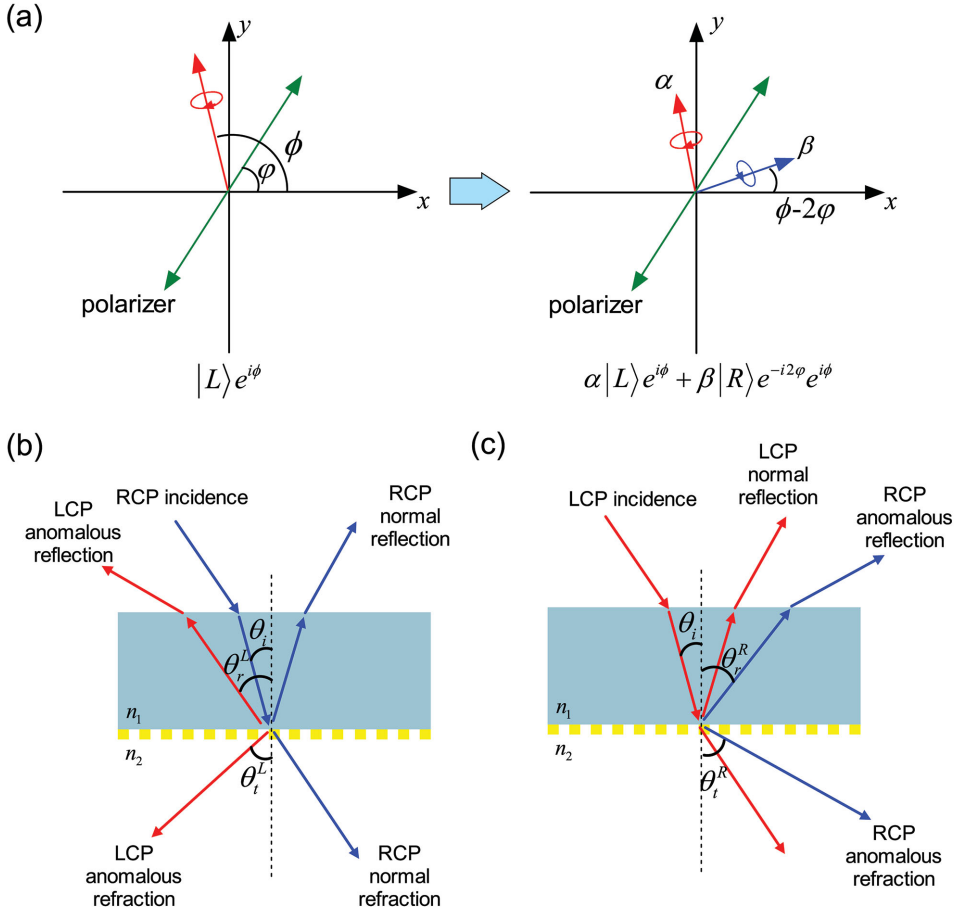

Figure 1. a) Schematic illustration of the imperfect linear polarizer. Left: A LCP incident light (red arrow line) with a phase angle ϕ interacts with the linear polarizer (green double-arrow line) with a rotation angle φ along x-axis; Right: linear polarizer could execute a mirror effect, which can symmetrically image the incident light to the opposite-helicity light with respect to the linear polarizer. The unconverted light (remained object) and converted light (image) have same amplitude ($\alpha = \beta = 0.5$) for a perfect linear polarizer, indicated by red and green arrow lines. Schematic illustrations of the normal and anomalous refraction and refection for b) RCP and c) LCP incident lights.

phase from 0 to 2π. The orientation angle can be expressed as $\varphi(x) = \pi x/L$, where L is the periodic length of the array. The transmitted light will be scattered in the different direction from that of the ordinary light, which has been known as the GSL of CP light. If the refractive indices for two media are n_1 and n_2, the relation between incident angle θ_i and anomalous angle θ_t can be written as (Supporting Information)

$$n_2 \sin\theta_t = n_1 \sin\theta_i + \sigma\frac{\lambda_0}{L} \tag{3}$$

where λ_0 is the wavelength in free space and $\sigma = \pm 1$ corresponds to the helicity of RCP and LCP incident light. The anomalous light has opposite helicity with that of the incident light as it is the image of the incident light. The helicity of normal light will be unchanged and obey the ordinary Snell's law. Figure 1b,c gives the schematic illustrations of the RCP and LCP incident lights, supposing that the linear polarizer has similar polarization effect in reflective side. According to Equations (1) and (2), the anomalous light has an amplitude of β, which is decided by the extinction capability of the linear polarizer in the perpendicular polarization direction. The ordinary and anomalous lights will have same amplitude ($\alpha = \beta = 0.5$) when the array of linear polarizers is perfect. As β is the intrinsic value for each polarizer, the orientation of polarizer will not affect the amplitude of converted image. However, if the polarizers have different values of β in a period, which can be realized by introducing different types of polarizers or by coupling of neighbor polarizers, the transmitted anomalous lights would contain not only one beam. In this case, the propagation direction for each beam can be derived by Fourier analysis.

A nanometallic antenna can be approximately regarded as an imperfect linear polarizer in both refractive and reflective sides. This is because it reduces the light intensity when the polarization is along with/perpendicular to the nanorod antenna in refractive/reflective side. The refractive light at the resonant frequency will be most efficiently scattered by the nanorod antenna; however, which is only a small part of radiated electromagnetic wave. Most of radiated electromagnetic wave is eliminated by the nanorod antenna. Meanwhile, the bandwidth of the scattered light is often narrow for the single-nanorod antenna, which limits the applications of the scattered light in many fields. Therefore, we presented a multinanorod metasurface to improve the efficiency and bandwidth of scattered light. **Figure 2**a shows the schematic diagram of the proposed multinanorod metasurface composed by eight multinanorod unit cells, which is linearly varied orientations with a step size of $\pi/8$ along the x-direction. Each unit cell consists of four identical gold nanorod with length l = 300 nm, width w = 50 nm, and thickness t = 50 nm. The space between two nanorods is d = 30 nm. The separated distance between each unit cell is 475 nm in both x- and y-directions. Thus, it repeats with a periodicity of 3800 nm in the x-direction and 475 nm in the y-direction.

We calculated the amplitude transmittance β of the anomalous refracted light for different multinanorod metasurfaces in Figure 2b. Results show that the bandwidth of the amplitude transmittance can be dramatically expanded by increasing the number of nanorod antenna in one unit cell. The maximum amplitude transmittance can be approximately reached at 0.5 in a broadband range, which is corresponding to the perfect linear polarizer. Meanwhile, the central frequency has a large blueshift compared with that of the single-nanorod metasurface.

The broadband and blueshift effects can be easily understood by the theory of radiation damping and plasmonic hybridization. It has been proved that the dephasing time of electrons determines the bandwidth of the plasmon resonance as light field excites oscillations in nanoparticles.[24] When near-field coupling occurs, the radiation damping is much larger than that of an isolated nanoparticle.[25,26] The radiation damping mainly contributes to broaden the bandwidth in the case of large nanoparticles. Therefore, the nanorods by setting together will broaden the bandwidth of the resonance frequency, while the amplitude transmittance β maintains higher across whole broadband range. More nanorods interacting in near-field will produce stronger coupling, and greatly increase the radiation damping. This is why the multinanorod metasurfaces as the linear polarizers perform better across large broadband range compared with same sized unit cell with less nanorod. The phenomenon that multinanorod metasurface pushes resonant wavelength toward short wavelength is mainly due to the hybridization of plasmon, as shown in **Figure 3**a. When a single nanorod is interacted with incident light, certain resonant frequency is found corresponding to an intrinsic oscillation state $|\omega\rangle$ with energy E. When two nanorods are set along with each other, coupling occurs and the initial state $|\omega\rangle$ is split into two other states $|\omega_+\rangle$ and $|\omega_-\rangle$ in higher and lower energy, which are respectively corresponding to the symmetrical and antisymmetrical modes.[27–30] However, our configuration only ensures symmetrical mode, so a slight blueshift can be observed. Similarly, more nanorods (e.g., four nanorods shown in Figure 3b) will have more coupling cases and greater eigenenergy splitting, which result in generating larger blueshift. The resonance of multinanorod

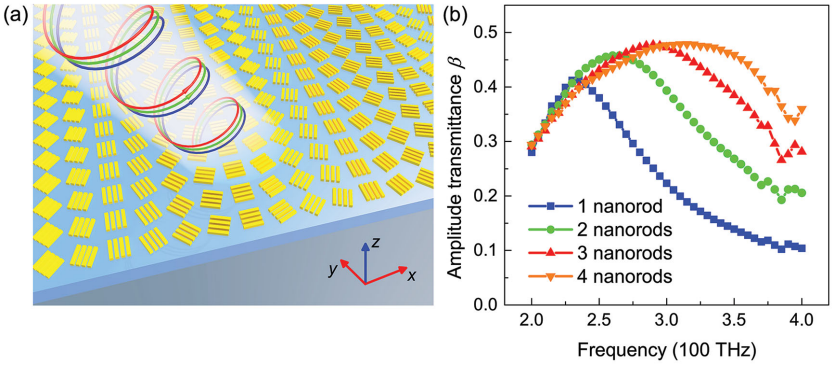

Figure 2. a) Schematic diagram of the high-performance broadband multinanorod metasurface composed by eight multinanorod unit cells, which is linearly varied orientations with a step size of $\pi/8$ along the x-direction. b) Calculated amplitude transmittance of the anomalous refracted light for different multinanorod metasurfaces. The bandwidth and central frequency of the amplitude transmittance can be dramatically expanded and shifted by increasing the number of nanorod antenna.

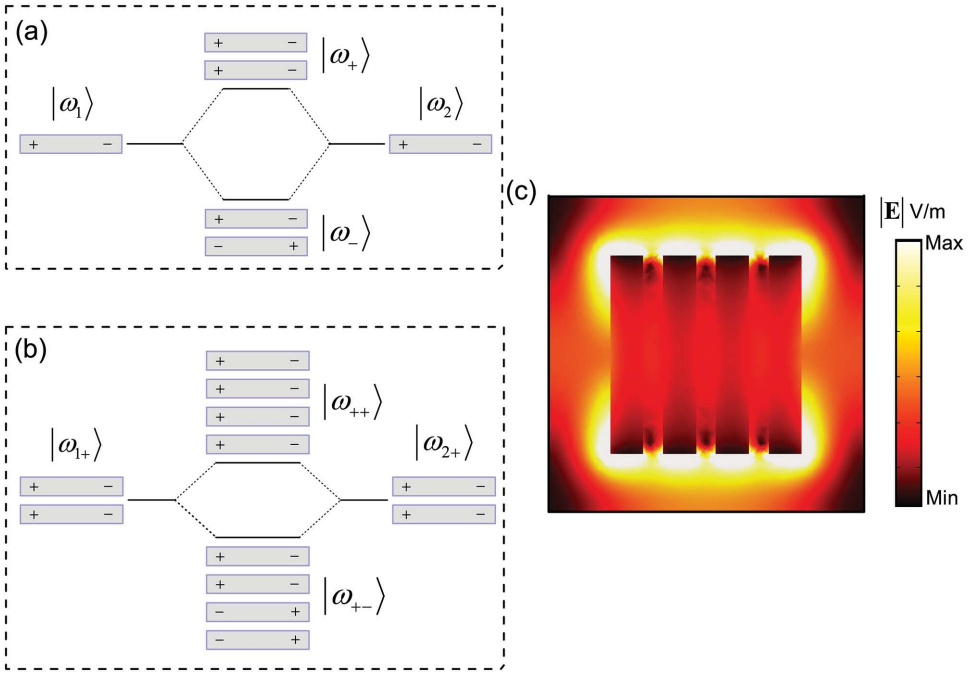

Figure 3. Schemes of plasmonic hybridization for a) two and b) four nanorods. When two nanorods with eigenstates $|\omega_1\rangle$ and $|\omega_2\rangle$ are coupling with each other, the initial state is split into higher energy state $|\omega_+\rangle$ (symmetrical mode) and lower energy state $|\omega_-\rangle$ (anti-symmetrical mode). Only symmetrical mode is available in our case. Four nanorods will have more coupling cases and more great eigenenergy splitting, and generate larger blueshift. c) Electric field distribution mode for four-nanorod metasurface when the polarization of the normally incident light is along with the nanorods at resonant frequency. Strong near-field couplings between the nanorods result in the effects of broadband and blueshift.

metasurface will therefore shift far away toward short wavelength compared with that of single nanorod. Figure 3c shows the electric field distribution mode for the multinanorod metasurface as incident light polarization is along with the nanorods at resonant frequency. The strong near-field couplings between the nanorods make sure that the radiation damping and hybridization are strongly enhanced. These effects result that the amplitude transmittance is significantly improved in a broadband range.

To demonstrate the broadband and high efficiency performance of our proposed multinanorod metasurface in the experiments, we fabricated four samples by the E-beam deposition and lithography, as shown in **Figure 4**a–d, which correspond to one-, two-, three-, and four-nanorod metasurface. Figure 4e gives the LCP/RCP anomalous refraction angle as a function of RCP/LCP incident angle for four-nanorod metasurface at 980 nm incident wavelength. The bright lines are the theoretical calculated anomalous refraction angles for both RCP and LCP incident according to Equation (3). The experimental results (triangle marks) are in very good agreement with the theoretical prediction. Besides, the anomalous refraction maintains high intensity across wide angle range even it approaches the required angle of evanescent wave. Figure 4f theoretically and experimentally proves the broadband effect of the four-nanorod metasurface when the LCP and RCP lights are normally incident. Similarly, the anomalous refraction angles in experiments fit the theoretical prediction quite well, and the intensity of the anomalous refraction light still keeps at high value throughout a broadband wavelength range. The fabricated multinanorod metasurfaces were characterized by performing far-field normalized transmission measurements as a function of the observation angle for normally incident CP light at 900 and 980 nm wavelengths, as shown in **Figure 5**. The measured anomalous refraction angles are consistent with our structural designs with anomalous refraction angles of 13.7° and 14.9° for 900 and 980 nm wavelengths, respectively. The fabricated multinanorod metasurfaces have uniform anomalous refraction angle at the fixed wavelength as they have same periodic length L = 3800 nm. However, the intensity of the anomalous refraction light scattered by the four plasmonic metasurfaces are quite different. The intensity of the anomalous refraction light is dramatically increased with the increasing of the number of the nanorods. Four-nanorod metasurface has the highest efficiency of generating anomalous refraction light for both of two measured wavelengths. Figure 5 shows that the transmission increases dramatically with the number of nanorods. However, it seems that the three-rod and four-rod configurations show similar efficiency in Figure 2b. One of the main reasons is the results in Figures 2b and 5 are the calculated amplitude and measured the intensity of the anomalous light, respectively. In addition, there is a redshift in the experimental results, which results in a slight different between the simulated and experimental results. The redshift in experiment is mainly induced by the difference between the simulated and measured refractive index for the substrate, and the undesired errors in fabrication.

An arbitrary incident light can be decomposed into two orthogonal CP lights with opposite helicity. The multinanorod metasurface exactly has the capability of scattering different helicity incident lights in a broadband wavelength range. **Figure 6**a schematically shows that our proposed multinanorod metasurface has the functionality of a polarized beam splitter

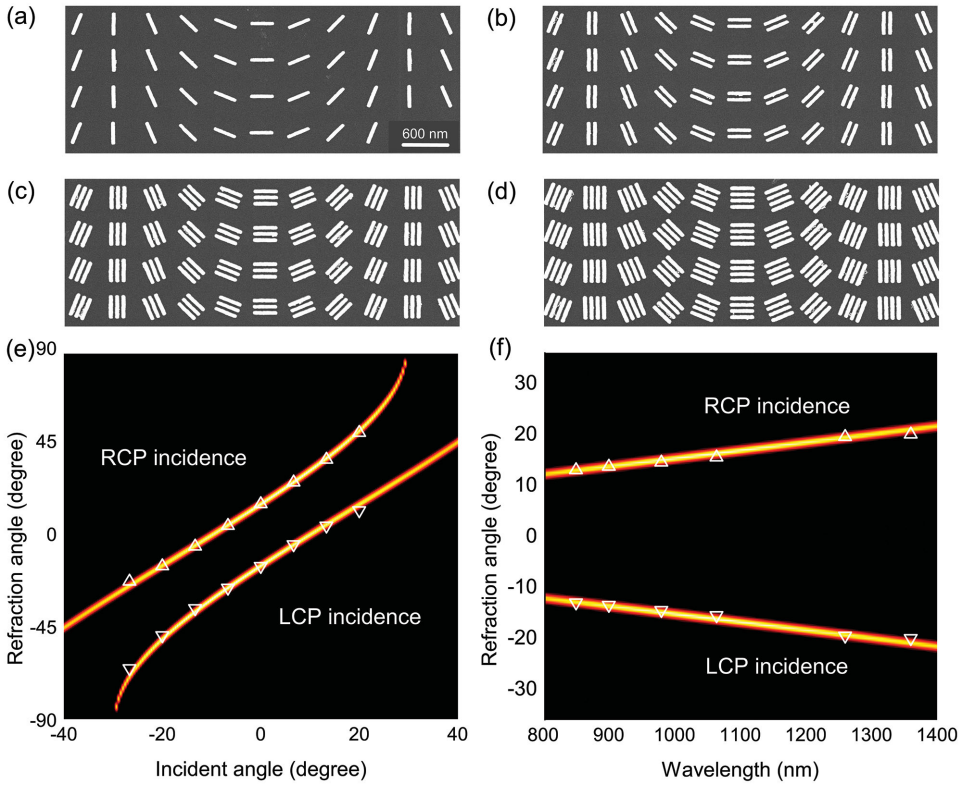

Figure 4. Scanning electron microscope (SEM) images of the fabricated a) one-, b) two-, c) three- and d) four-nanorod metasurface. Experimentally measured (triangle marks) and theoretical calculated (bright lines) anomalous refraction angles as a function of e) RCP/LCP incident angle for 980 nm incident wavelength and f) RCP/LCP incident wavelength for normal incidence for four-nanorod metasurface. The intensity of the anomalous refraction light maintains high across wide angle and broadband wavelength range.

and can be used to split the non-CP incident light in broadband range. The anomalous lights refracted in two directions are CP, and their amplitude is determined by the polarization of incident light. We assume an arbitrary polarized incident light is denoted by Jones vectors as $E_i = \begin{bmatrix} A \\ Be^{i\delta} \end{bmatrix}$, whose polarization is indicated by the x- and y-amplitude components (A and B) as well as their phase difference δ. According to the operators in Equations (1) and (2), the anomalous scattered lights have the amplitudes as follows:

$$a_L = \frac{\beta}{4}\sqrt{1+\frac{2AB}{A^2+B^2}\sin\delta} \tag{4}$$

$$a_R = \frac{\beta}{4}\sqrt{1-\frac{2AB}{A^2+B^2}\sin\delta} \tag{5}$$

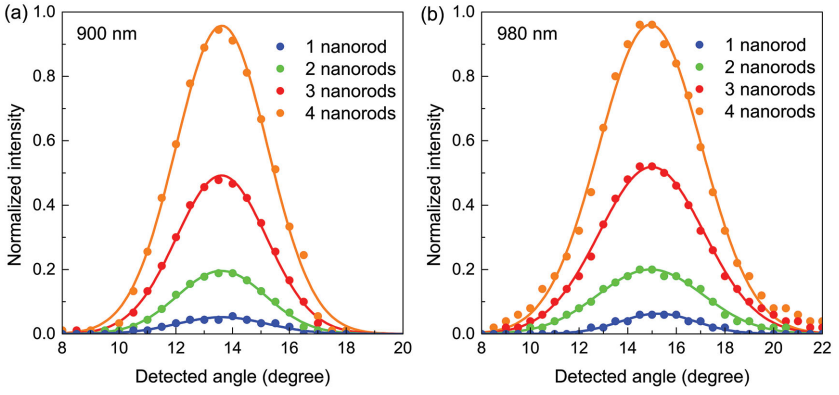

Figure 5. Far-field normalized transmission measurements (solid circles) and Gaussian fitting (solid lines) for anomalous refraction light as a function of the observation angle for normally incident CP light at a) 900 nm and b) 980 nm wavelengths. Four-nanorod metasurface has the highest efficiency of generating anomalous refraction light.

where a_L and a_R denote the amplitudes of LCP and RCP anomalous lights. When incident light is linearly polarized, equal amplitude of LCP and RCP light could be obtained. Figure 6b gives the experimental and theoretical normalized intensity of LCP and RCP anomalous refraction lights as the changing of the polarization of incident light for normal incidence at 980 nm wavelength. A quarter wave plate (QWP) before the sample was rotated from 0 to π to experimentally change the polarization of incident light. When the angle of QWP is set to be 45° or 135°, the polarization of the incident light is linearly polarized. The detected LCP and RCP anomalous refraction lights have same intensity following the foregoing discussion in

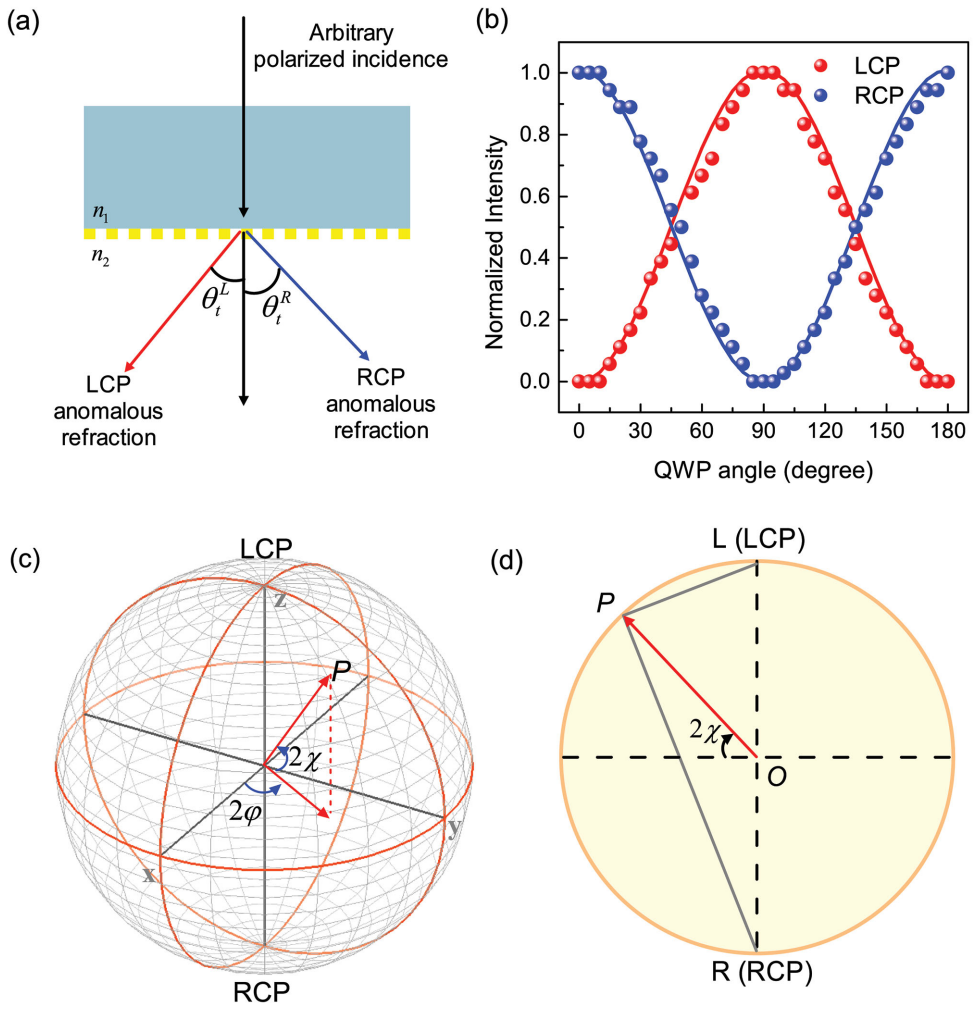

Figure 6. a) Schematic illustration of the functionality of a polarized beam splitter for the multinanorod metasurface, which can be used to split the non-CP incident light in broadband range. b) Experimental (balls) and theoretical (solid lines) normalized intensity of LCP and RCP anomalous refraction lights as the rotation of the QWP angle for normal incidence at 980 nm wavelength. c) An arbitrary polarization $P(2\varphi,2\chi)$ on Poincaré sphere and d) its great circle across this arbitrary polarization P. The scattered amplitudes for LCP and RCP anomalous refraction lights are inversely proportional to the lengths of the PL and PR.

Equations (4) and (5). Apparently, the incident linearly polarized light can be easily split into LCP and RCP anomalous refraction lights with large refraction angle and high efficiency by the proposed multinanorod metasurface. The polarization of the incident light will be LCP or RCP when the angle of QWP is 0° or 180°. The total anomalous refraction light will only have RCP or LCP component. Again, the experimental results (balls) are in good agreement with the theoretical prediction (solid lines).

According to Equations (4) and (5), the ratio of a_L/a_R is a constant for any polarization state of incident light, where the parameter β associated with the property of nanorod is eliminated. Whether the linear polarizer is perfect or not, the polarization state of incident light is always determined by the ratio of a_L/a_R. This characteristic can also be reflected on Poincaré sphere. Figure 6c presents an arbitrary polarization $P(2\varphi,2\chi)$ on Poincaré sphere, whose north and south pole refer to LCP and RCP states. The great circle across arbitrary polarization P is subsequently given in Figure 6d. An arbitrary incident light can be regarded as the combination of LCP and RCP lights, and their amplitudes are proportional to the lengths of the PL and PR in Figure 6d. However, after the incident light interacts with the multinanoraod metasurface, the scattered amplitudes for LCP and RCP anomalous refraction lights are inversely proportional to the lengths of the PL and PR in Figure 6d (Supporting Information). The underlying reason is that the anomalous lights are the image of incident light, and they have opposite helicity compared with the incident light. These properties supply us a convenient method to quickly determine the polarization point on Poincaré sphere for the incident light. Meanwhile, they also provide an easy way to detect the polarization degree of the incident light once a_L/a_R is determined.

3. Conclusion

In summary, we have proposed an easy and intuitive way to describe the function of polarizer. We designed and fabricated

the multirod metasurfaces, which are able to deflect light with an extraordinarily broadband and high efficiency. The correctness of GSL is also demonstrated in experiments. We investigated the cases of the arbitrary polarized incident light, and gave the amplitude ratio for two scattered beams. The demonstration is in the near-infrared wavelength range, which indicates that the approach can be easily translated to mid-infrared, terahertz, and microwave frequency regimes. Our work can lead to many applications, such as polarization beam splitters, polarization detector. Due to its broadband, high efficiency and polarization property, information coding and decoding are also a promising application in optic communication in the future.

4. Experimental Section

Sample Fabrication: Electron-beam lithography, metal evaporation, and lift-off process were used to fabricate the metallic structures. The samples shown in Figure 4 for the anomalous refraction were fabricated using the following steps. 200 nm thick polymethyl methacrylate (PMMA) resist was spin-coated on glass substrate, and then baked at 180 °C on a hot plate for 2 min. The pattern was exposed using an electron-beam lithography system (JBX-6300FS) at 100 keV, followed by developing in methyl isobutyl ketone (MIBK) : iso propyle alcohol (IPA) (1:3) for 40 s and IPA for 30 s. Then 5 nm Cr and 50 nm Au film was deposited onto the sample by electron beam evaporation. The Cr layer here aimed to increase the adhesion between Au film and substrate. Then, the sample was immersed into acetone to fully resolve the resist, leaving the metal pattern on substrate.

Measurement Setup for the Anomalous Refraction: A series of semiconductor laser were used to provide laser pulses with a central wavelength of 850, 900, 980, 1064, 1260, and 1360 nm, respectively. An aperture was used to adjust the spot diameter. A polarizer and a series of quarter-wave plate for a fixed wavelength were combined to generate the incident circularly polarized light, which was focused on the sample with a 20×/0.40 NIR microscope objective. The transmission light through the sample was collected by using a lens. For the refractive angle detection, we used two-concentric-rotary system to achieve independent rotation of the sample orientation and the detector angle. The resolution of the rotation system was 0.02°. The lens, analyzer, and power meter in the rotary system were used to measure the intensity of the anomalous light. The analyzer which is still composed of a quarter-wave plate for a fixed wavelength and a polarizer was inserted into the optical path to analyze the polarization status of the anomalous light. The other rotary stage was used to adjust the orientation of the sample for oblique incident while the position of the sample was maintained at the center of the stage. This setup allowed us to verify the anomalous refraction phenomenon generated by the sample. Moreover, the optical elements, including the microscope objective, lens, polarizer, and detector, were operated in the broadband range.

Supporting Information

Supporting Information is available from the Wiley Online Library or from the author.

Acknowledgements

Zhaocheng Liu and Z. Li contributed equally to this work. This work was supported by the National Basic Research Program (973 Program) of China (2012CB921900), the Chinese National Key Basic Research Special Fund (2011CB922003), the Natural Science Foundation of China (61378006, 11304163, 11174362, and 91323304), the Program for New Century Excellent Talents in University (NCET-13-0294), the Natural Science Foundation of Tianjin (13JCQNJC01900), the International Science and Technology Cooperation Program of China (2013DFA51430), the 111 project (B07013), and the National Science Fund for Talent Training in Basic Sciences (J1103208).

Received: May 18, 2015
Revised: June 20, 2015
Published online: July 27, 2015

[1] N. Yu, P. Genevet, M. A. Kats, F. Aieta, J. P. Tetienne, F. Capasso, Z. Gaburro, *Science* **2011**, *334*, 333.
[2] F. Aieta, P. Genevet, N. Yu, M. A. Kats, Z. Gaburro, F. Capasso, *Nano Lett.* **2012**, *12*, 1702.
[3] N. Yu, F. Capasso, *Nat. Mater.* **2014**, *13*, 139.
[4] X. Zhang, Z. Tian, W. Yue, J. Gu, S. Zhang, J. Han, W. Zhang, *Adv. Mater.* **2013**, *25*, 4566.
[5] M. Farmahini-Farahani, H. Mosallaei, *Opt. Lett.* **2013**, *38*, 462.
[6] S. Sun, K.-Y. Yang, C.-M. Wang, T.-K. Juan, W. T. Chen, C. Y. Liao, Q. He, S. Xiao, W.-T. Kung, G.-Y. Guo, L. Zhou, D. P. Tsai, *Nano Lett.* **2012**, *12*, 6223.
[7] A. Pors, M. G. Nielsen, R. L. Eriksen, S. I. Bozhevolnyi, *Nano Lett.* **2013**, *13*, 829.
[8] A. Pors, O. Albrektsen, I. P. Radko, S. I. Bozhevolnyi, *Sci. Rep.* **2013**, *3*, 2155.
[9] Y. Yang, W. Wang, P. Moitra, I. I. Kravchenko, D. P. Briggs, J. Valentine, *Nano Lett.* **2014**, *14*, 1394.
[10] P. Genevet, N. Yu, F. Aieta, J. Lin, M. A. Kats, R. Blanchard, M. O. Scully, Z. Gaburro, F. Capasso, *Appl. Phys. Lett.* **2012**, *100*, 013101.
[11] N. Yu, F. Aieta, P. Genevet, M. A. Kats, Z. Gaburro, F. Capasso, *Nano Lett.* **2012**, *12*, 6328.
[12] J. Li, S. Chen, H. Yang, J. Li, P. Yu, H. Cheng, C. Gu, H.-T. Chen, J. Tian, *Adv. Funct. Mater.* **2014**, *25*, 704.
[13] L. Huang, X. Chen, H. Mühlenbernd, G. Li, B. Bai, Q. Tan, G. Jin, T. Zentgraf, S. Zhang, *Nano Lett.* **2012**, *12*, 5750.
[14] L. Huang, X. Chen, H. Mühlenbernd, H. Zhang, S. Chen, B. Bai, Q. Tan, G. Jin, K. W. Cheah, C.-W. Qiu, J. Li, T. Zentgraf, S. Zhang, *Nat. Commun.* **2013**, *4*, 2808.
[15] X. Chen, L. Huang, H. Mühlenbernd, G. Li, B. Bai, Q. Tan, G. Jin, C.-W. Qiu, S. Zhang, T. Zentgraf, *Nat. Commun.* **2012**, *3*, 1198.
[16] M. Kang, T. Feng, H.-T. Wang, J. Li, *Opt. Express* **2012**, *20*, 15882.
[17] D. Lin, P. Fan, E. Hasman, M. L. Brongersma, *Science* **2014**, *345*, 298.
[18] N. K. Grady, J. E. Heyes, D. R. Chowdhury, Y. Zeng, M. T. Reiten, A. K. Azad, A. J. Taylor, D. A. R. Dalvit, H.-T. Chen, *Science* **2013**, *340*, 1304.
[19] H.-T. Chen, J. Zhou, J. F. O'Hara, F. Chen, A. K. Azad, A. J. Taylor, *Phys. Rev. Lett.* **2010**, *105*, 073901.
[20] F. Monticone, N. M. Estakhri, A. Alù, *Phys. Rev. Lett.* **2013**, *110*, 203903.
[21] N. Engheta, A. Salandrino, A. Alù, *Phys. Rev. Lett.* **2005**, *95*, 095504.
[22] Z. Liu, S. Chen, J. Li, H. Cheng, Z. Li, W. Liu, P. Yu, J. Xia, J. Tian, *Opt. Lett.* **2014**, *39*, 6763.
[23] F. Gori, *Opt. Lett.* **1999**, *24*, 584.
[24] G. V. Hartland, *Chem. Rev.* **2011**, *111*, 3858.
[25] C. Dahmen, B. Schmidt, G. V. Plessen, *Nano Lett.* **2007**, *7*, 318.
[26] P. Olk, J. M. Renger, T. Wenzel, L. M. Eng, *Nano Lett.* **2008**, *8*, 1174.
[27] E. Prodan, C. Radloff, H. J. Halas, P. Nordlander, *Science* **2003**, *302*, 419.
[28] N. Liu, H. Guo, L. Fu, S. Kaiser, H. Schweizer, H. Giessen, *Adv. Mater.* **2007**, *19*, 3628.
[29] V. T. T. Thuy, D. T. Viet, N. V. Hieu, Y. P. Lee, V. D. Lam, N. T. Tung, *Opt. Commun.* **2010**, *283*, 4303.
[30] B. Kanté, S. N. Burokur, A. Sellier, A. D. Lustrac, J. M. Lourtioz, *Phys. Rev. B* **2009**, *79*, 07512.